

# Underwater Image Denoising Based on Curved Wave Filtering and Two-dimensional Variational Mode Decomposition

Lin Teng<sup>1</sup>, Yulong Qiao<sup>1,\*</sup>, and Shoulin Yin<sup>1,2</sup>

<sup>1</sup> School of Information and Communication Engineering, Harbin Engineering University  
145 Nantong Street, Nangang District, Harbin City and 150001, China  
qiaoyulong@hrbeu.edu.cn

<sup>2</sup> Software College, Shenyang Normal University  
Shenyang, 110034 China  
yslin@hit.edu.cn

**Abstract.** Underwater image denoising technology is of great significance in underwater operation. Underwater operations (such as offshore oil drilling, under-sea tunnels, pipeline construction, underwater archaeology, biological research, and lifesaving) require stable and clear underwater images to aid analysis. Due to the scattering and absorption of light by water bodies, obtaining high-quality underwater images is a challenging task. Underwater images are prone to low contrast, low resolution and edge distortion. Therefore, it is difficult to accurately separate the effective signal when removing the underwater image noise, which leads to the image contrast reduction. Also the edge contour is not clear, and the detail loss is serious. Therefore, we propose a novel underwater image denoising method based on curved wave filter and two-dimensional variational mode decomposition. Firstly, the noisy image is decomposed by two-dimensional variational mode decomposition, and a series of modal components with different center frequencies are obtained. The effective modal components are selected by correlation coefficient and structural similarity. And the effective modal components are processed by the curve-wave filter. Finally, the filtered modal components are reconstructed to remove the noise in the image. The experimental results show that, compared with other state-of-the-art methods, the proposed method has clearer denoising results, less mean square error, and better denoising effect.

**Keywords:** Underwater image denoising, curved wave filter, two-dimensional variational mode decomposition, image reconstruction.

## 1. Introduction

With the rapid development of science and technology, human beings need to further develop Marine resources and understand the seabed organisms and available resources, which will be conducive to the study of Marine resources. As an auxiliary means of underwater vision, clear underwater images are the most intuitive way to understand the underwater world [1-3]. Although there is a high-quality imaging system for remotely operated underwater vehicles, due to the dispersion of water molecules, microorganisms in water,

---

\* Corresponding Author

and the quality of sensing elements in the camera, the underwater images collected will contain a lot of complex noise, which greatly reduces the visual quality of underwater images. It seriously affects the application of machine vision and late underwater images, and brings great challenges to the field of computer vision [4,5].

As a kind of water resources, Marine resources play a very important role in the development of human society and the earth's energy cycle [6]. Different from the terrestrial environment, the complexity, variability and dynamics of the Marine environment bring serious challenges to underwater exploration [7]. Underwater image denoising technology is an early means of ocean exploration, and plays an important role in seabed topography mapping, underwater target object recognition and detection, and biological population monitoring [8,9]. Due to the presence of scatterers in the ocean and the reverberation effect caused by the undulating seafloor and sea surface, the image has serious speckled noise, especially in the shallow sea area [10]. Speckled noise and interfering signals lead to degraded image quality, which adversely affects subsequent image processing. Therefore, the study of underwater image denoising method has always been the focus of research [11].

Classical image denoising methods include mean filter [12], median filter [13], wavelet transform [14], etc. Although the above denoising methods are simple in operation and have strong adaptability, there are unavoidable problems. Although mean filter is fast in calculation, it will damage the high frequency region of the image in the process of denoising, resulting in the loss of image details. Median filtering replaces the central pixel value of the window with the middle value after sliding window sorting, which can remove the noise in the high frequency part of the image. However, for the part of the image with relatively dense noise, the denoising effect of median filtering will be weakened, and the image will become blurred with the increase of sliding window. These methods need to adjust the filter suitable for the noise characteristics according to the local noise, which is faced with many difficulties. In the wavelet transform, the selection of the threshold will affect the denoising effect of the image. In addition, different noise images need to set different thresholds.

Different threshold functions in the curve-wave threshold denoising framework [15] produce different denoising effects. The soft threshold and hard threshold functions described in references [16,17] had been widely used, but they had different degrees of defects. The discontinuity of the curve wave hard threshold function at the threshold point caused obvious visual distortion such as ringing and pseudo-Gibbs effect in de-noised images. There is a constant deviation between the curve coefficients before and after the soft threshold function processing, which leads to the blur of the edge of the image and the decrease of the visual quality of the de-noised image. Therefore, the construction of an efficient threshold function is the key to improve the de-noising performance of the curve-wave threshold de-noising method [18]. In addition, the curve-wave threshold denoising method can only ensure that the noise whose absolute value is less than the threshold value is removed, and there is no unified standard for the selection of threshold values. Surround effect will occur, resulting in poor image visual quality [19]. In view of these inherent performance defects of the wavelet threshold denoising method, researchers will use Partial Differential Equation (PDE)[20] based on information fusion to improve the denoising effect of the wavelet threshold method [21].

In 2014, Dragomiretskiy et al. [22] proposed a completely non-recursive variational mode decomposition model (VMD), which could adaptively decompose the signal into a set of band-limited inherent mode functions and obtain the optimal value of the inherent mode function, thus solving problems such as the sensitivity of empirical mode decomposition to noise and sampling. In order to facilitate the processing of two-Dimensional signals, Dragomiretskiy et al. [23] proposed a two-dimensional variational mode decomposition model (2D-VMD) based on the VMD algorithm. The model was a natural two-dimensional extension in the context of image segmentation and orientation, and was a non-recursive, fully adaptive variational method that could decompose an image into a series of sub-modal components with different center frequencies. Many scholars have applied the 2D-VMD model to different areas of image processing. Zhang et al. [24] proposed a denoising method for medical ultrasound images based on two-dimensional variational mode decomposition combined with fast non-local mean, which could retain edge information well while denoising, and had a good denoising effect in high noise variance. Meriem et al. [25] used two-dimensional variational mode decomposition to reduce the random noise of fringe patterns and improve contour and residual images, thereby controlling and reducing the existence of defect flatness on the surface. Although some denoising algorithms based on two-dimensional variational mode decomposition have been proposed successively, no more effective denoising methods have been proposed according to the characteristics of underwater images.

Compared with other filtering methods, curve-wave filtering has a better effect on preserving image edge information and details in the process of denoising. Therefore, an underwater image denoising method combining wave-wave and two-dimensional variational mode decomposition is proposed in this paper. Firstly, the noisy image is decomposed into a series of modal components with different center frequencies by two-dimensional variational mode decomposition. Then, the correlation coefficient (CC) and structural similarity (SSIM) are used to select the effective modal components, and the effective modal components are processed by curvewave filtering. Finally, the filtered modal components are reconstructed to remove the noise in the image.

This paper has the following organization structure. In section 2, we introduce the Fast Discrete Curvelet Transform (FDCT). Section 3 detailed shows the proposed underwater image denoising. Experiments are conducted in section 4. There is a conclusion in section 5.

## 2. Fast Discrete Curvelet Transform (FDCT)

The Curvelet Transform (CT) [26,27] is decomposed on all possible scales using the Multi-scale Ridgelet Transform, the implementation of CT can be summarized as follows.  $I$  is the given dimension  $N \times N$  two-dimensional digital image signal, and its signal is decomposed by  $J$ -th layer binary wavelet, it can obtain:

$$I = C_j + \sum_{j=1}^J D_j \quad (1)$$

Where  $C_j$  is the low frequency component on the coarsest scale.  $D_{j, j=1,2,\dots,J}$  is the high frequency. The size value of  $j = 1, 2, \dots, J$  represents the thickness of the scale. The CT transformation process is shown in Figure 1.

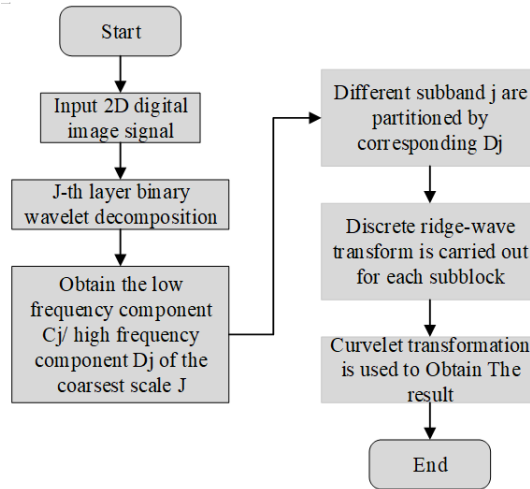


**Fig. 1.** The process of CT

**Table 1.** Approximation order under different transformations

Class	Approximation order
Fourier	$\ g - \bar{g}_m\ _2^2 = o(m^{-0.5})$
Wavelet	$\ g - \bar{g}_m\ _2^2 = o(m^{-1})$
Curvelet	$\ g - \bar{g}_m\ _2^2 = o(m^{-2})$

CT is a non-adaptive multi-scale geometric analysis method. Different from the adaptive method, CT does not need to know the geometric features of the image in priori, but does directly decompose the signal on a set of fixed frames or basis functions, and makes full use of the information of the function itself. It can use different kinds of function transformation for different parts of the image, so that the corresponding function types can achieve the optimal approximation, and provide a powerful "sparse" description of the image. Obviously, compared with the curve described by wavelet transform, CT breaks through the limitation of Govitch anisotropy of wavelet "sparse" expression signal [28]. The following theorem gives an optimal explanation of the Curvelet transformation.

Let  $f \in W_2^2(R^2)$  and  $g(x) = f(x)_{x_2 \leq \tau(x_1)}$ . If the curve  $\tau$  satisfies the second derivative, then the error order of the  $M$  term of the function  $g$  CT can be achieved by nonlinear approximation  $Q_M^2(g)$  is:

$$\|g - Q_M^C\|_2^2 \leq CM^2(\log M)^{0.5} \tag{2}$$

For second-order differentiable functions, it can be seen from  $(\log M)^{0.5}$  term that CT has almost reached the optimal approximation order, and its optimal approximation order is  $O(M^{-2})$ . The nonlinear wavelet transform approximation error decays at  $M^{-1}$  order. Table 1 shows the approximation order of function  $g$  under three different transformations (Fourier, Wavelet, Curvelet).

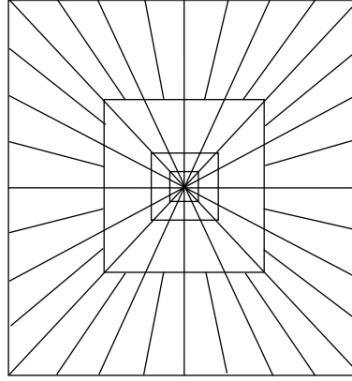


**Fig. 2.** Scale and Angle segmentation of discrete Curvelet transform

In order to realize the Curvelet transformation of two-dimensional discrete images without changing the construction frame of Curvelet, it is necessary to replace the ring wedge window function  $U_j$  with the square window function in two-dimensional Cartesian coordinate system, and use the center square region to describe the frequency domain segmentation of the discrete Curvelet transformation [29], as shown in Figure 2.

In a two-dimensional Cartesian coordinate system, we set the local window to  $\tilde{W}_j(\varpi) = \tilde{V}_j(\varpi)U_j(\varpi)$ , where  $j \geq 0$ , and,

$$\tilde{V}_j(\varpi) = \sqrt{\varphi_{j+1}^2 - \varphi_j^2} \quad (3)$$

$$U_j(\varpi) = U(2^{j/2}\varpi_2/\varpi_1) \quad (4)$$

Where,  $\varphi$  is the inner product of two one-dimensional low-pass Windows.

$$\varpi_j(\varphi_1, \varphi_2) = \phi(2^{-j}\varphi_1)\phi(2^{-j}\varphi_2) \quad (5)$$

With the frequency domain segmentation diagram above, it can be seen that the intervals of the curved wave transform segmentation are the same, and each interval has the same slope  $\tan \theta_1$ , and  $\tan \theta_1 = l \cdot 2^{-l/2}$ , where  $l = -2^{-j/2}, \dots, -2^{-j/2} - 1$ , then,

$$\tilde{W}_{j,l}(\varpi) = V_j(\varpi)U_j(\Gamma_{\theta_l}\varpi) \quad (6)$$

Where, the shear moment  $\Gamma_{\theta_l}$  is:

$$\begin{pmatrix} 1 & 0 \\ -\tan \theta & 1 \end{pmatrix} \quad (7)$$

Then a discrete Curvelet can be defined as:

$$\tilde{\mathfrak{R}}_{j,l,k}(x) = 2^{3j/4}\tilde{\mathfrak{R}}_j(\Gamma_{\theta_l}^T(x - \Gamma_{\theta_l}^{-T}b)) \quad (8)$$

$$b = (k_1 \cdot 2^{-j/2}, k_1 \cdot 2^{-j/2}) \quad (9)$$

The definition of the Curvelet transform is given by the following formula:

$$c(j, l, k) = \int \hat{g}(\varpi) \tilde{W}_j(T_{\theta_l}^{-1}) e^{i(T_{\theta_l}^{-1} b, \varpi)} d\varpi \quad (10)$$

In this paper, a simple and fast Unequally Spaced Fast Fourier Transform (USFFT) in CT transform is used for image filtering. The process of USFFT is shown in **Algorithm 1**.

---

**Algorithm 1** USFFT
 

---

- 1: Step 1: Transform the function  $g[t_1, t_2] \in L^2(R)$  by 2DFFT Fourier transform to obtain the Fourier sampling set  $\hat{g}[n_1, n_2]$ , where  $-n/2 \leq n_1, n_2 \leq n/2$ ;
  - 2: Step 2: In the frequency domain, re-sampling  $\hat{g}[n_1, n_2]$  on all scale and angular direction parameters  $(a, b)$  by interpolation method, get  $\hat{g}[n_1, n_2 - n_1 \tan \theta_b]$ , where  $(n_1, n_2) \in P_a$ ;
  - 3: Step 3: Multiply  $\hat{g}[n_1, n_2 - n_1 \tan \theta_b]$  with the fitting parabolic window  $\tilde{U}[n_1, n_2]$  and localize to get  $\hat{g}[n_1, n_2] = \hat{g}[n_1, n_2 - n_1 \tan \theta_b] \times \tilde{U}[n_1, n_2]$ . Among them, the fitting window size satisfies  $width = length^2$ ;
  - 4: Step 4: Transform the localization  $\hat{g}[n_1, n_2]$  into a 2DIFFT inverse Fourier transform to obtain the Curvelet transformation coefficient  $c^D(a, b, k)$ ;
- 

### 3. Proposed Underwater Image Denoising

The variational mode decomposition (VMD) algorithm can decompose the signal into a set of component modes with specific direction and oscillation characteristics. These intrinsic mode functions can accurately reconstruct a given input signal while limiting each mode to an online estimated center frequency. Based on the successful application of VMD algorithm in one-dimensional signal decomposition, researchers naturally extended VMD algorithm on two-dimensional signals and proposed two-dimensional variational mode decomposition, which was more suitable for two-dimensional image decomposition. Compared with variational mode decomposition, two-dimensional variational mode decomposition minimizes the bandwidth of the sub-signal while maintaining data fidelity [30].

In one-dimensional analytic signals, the signal is analyzed through a single side spectrum, so the negative frequency needs to be set to zero. Generalizing a one-dimensional analytic signal to a two-dimensional analytic signal requires effectively setting to zero half of the plane of the frequency domain, which corresponds to a vector denoted  $w_k$ . Therefore, the two-dimensional analytic signal is defined as follows in the frequency domain:

$$D_{AS,k}(w) = \begin{cases} 2u_k(w) & (w, w_k) > 0 \\ u_k(w) & (w, w_k) = 0 \\ 0 & (w, w_k) < 0 \end{cases} \quad (11)$$

$$u_{AS,k}(x) = u_k(x) * \left( \delta(\langle x, w_k \rangle) + \frac{j}{\pi \langle x, w_k \rangle} \right) \times \delta(\langle x, w_{k,\perp} \rangle) \quad (12)$$

Here,  $*$  denotes convolution, transformations are separable.

The analysis signal  $w_k$  is computed linearly along the reference direction and is processed independently, so the definition is one-dimensional in nature, but has the desired two-dimensional Fourier properties.

The function of 2D-VMD is determined according to the components of generalized variational mode decomposition. The formula for the minimization of the function is as follows:

$$\begin{aligned} \min_{u_k, w_k} \sum_k \alpha_k \|\nabla[u_{AS,k}(x)e^{-j\langle w_k, x \rangle}]\|_2^2 \\ \text{s.t. } \forall x : \sum_k u_k(x) = f(x) \end{aligned} \quad (13)$$

The constraints are reconstructed by quadratic punishment and augmenting Lagrange function, and optimized by multiplication operator alternate direction method (ADMM) [14].

As with the one-dimensional analytic signal, the  $u_k$  of the two-dimensional analytic signal is optimized:

$$\begin{aligned} u_k^{n+1} = \underset{u_k}{\operatorname{argmin}} \alpha_k \|\nabla[u_{AS,k}(x)e^{-j\langle w_k, x \rangle}]\|_2^2 \\ + \underset{u_k}{\operatorname{argmin}} \|f(x) - \sum_i u_i(x) + \lambda(x)/2\|_2^2 \end{aligned} \quad (14)$$

The following Wiener filter result will be produced:

$$\begin{aligned} u_k^{n+1}(w) = (f(w) - \sum_{i \neq k} u_i(w) + \lambda(w)/2) \\ \times \frac{1}{1 + 2\alpha_k |w - w_k|^2} \end{aligned} \quad (15)$$

Where  $\forall w \in \Omega_k : \Omega_k = w | (w, w_k) \geq 0$ . The center frequency  $w_k$  is slightly simpler to optimize, and its update goal is:

$$w_k^{n+1} = \underset{w_k}{\operatorname{argmin}} \alpha_k \|\nabla[u_{AS,k}(x)e^{-j\langle w_k, x \rangle}]\|_2^2 \quad (16)$$

The first moment of the power spectrum  $|u_k(w)|^2$  on the half plane  $\Omega_k$  model is:

$$w_k^{n+1} = \frac{\int_{\Omega_k} w |u_k(w)|^2 dw}{\int_{\Omega_k} |u_k(w)|^2 dw} \quad (17)$$

According to equations (14) and (16),  $K$  intrinsic modal components of the two-dimensional analytic signal are obtained.

Before the inverse Fourier transformation results are obtained, data needs to be constantly updated in the frequency domain. The specific process of the 2D-VMD can be described as in **Algorithm 2**:

Therefore, the flowchart of proposed underwater image denoising is shown in figure 3. The denoising algorithm proposed in this paper is shown in **Algorithm 3**.

**Algorithm 2** 2D-VMD

- 
- Step 1: Initializing the parameters  $w_k^0, u_k^0, \lambda^0$ , and  $n = 0$ ;  
 2: Step 2: Set the iteration  $n = n + 1$  and update  $u_k, w_k$ . The  $u_k$  and  $w_k$  are updated as follows:

$$w_k^{n+1} = \frac{\int_{\mathbb{R}^2} w |u_{AS,k}^{n+1}(w)|^2 dw}{\int_{\mathbb{R}^2} |u_{AS,k}^{n+1}(w)|^2 dw} \quad (18)$$

$$u_k^{n+1}(x) = \Re F^{-1} u_{AS,k}^{n+1}(w) \quad (19)$$

- Step 3: Update multiplication operator  $\lambda$  as follows:

$$\lambda^{n+1}(w) = \lambda^n(w) + \tau(f(w) - \sum_k u_k^{n+1}(w)) \quad (20)$$

$\tau$  indicates the step update coefficient.

- 4: Step 4: Determine whether the component satisfies the constraint condition  $\frac{\sum_k \|u_k^{n+1} - u_k^n\|_2^2}{\|u_k^n\|_2^2} < K_\epsilon$ . If satisfy it, stop iteration; If not, go back to Step 2) and continue iterating;
- 

**Algorithm 3** Proposed denoising algorithm

- 
- Step 1: A series of IMF images with different center frequency modal components are obtained by using 2D-VMD algorithm;  
 Step 2: The correlation coefficient and structural similarity are used to screen the series of modal components, and the modal components are divided into effective IMF image components and ineffective IMF image components;  
 3: Step 3: The image component of the effective IMF is filtered by the curvilinear filter, and the effective modal component after filtering is obtained;  
 Step 4: The effective modal components after filtering are reconstructed and the denoised images are obtained;
-

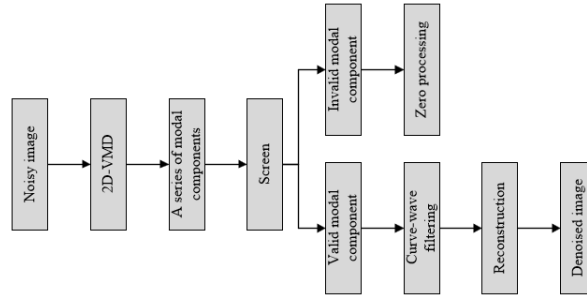


**Fig. 3.** The whole process of denoising.

#### 4. Experiments and Analysis

Some underwater images are randomly selected from the dataset UIEB [31] as experimental images, as shown in Figure 4. The peak signal-to-noise ratio (PSNR) [32] and structural similarity (SSIM) [33] are used as measurement indexes. The experimental environment is Windows11, CPU i510400F, and memory 16GB, 3th Gen Intel(R) Core(TM) i5-13400F 2.50 GHz. At the same time, we compare with the reference TVM [34], WTM [35] and MSRG [36].

PSNR, as an objective criterion for image evaluation, mainly calculates the degree of distortion between the processed image and the real image. The larger value denotes that the denoised image is more similar to the real underwater image. The calculation of MSE and PSNR is shown in equation (21) and equation (22):

$$MSE(x, y) = \frac{1}{M \times N} \sum_{i=1}^H \sum_{j=1}^W (W(i, j) - Y(i, j))^2 \quad (21)$$

$$PSNR(x, y) = 10 \times \lg\left(\frac{M_{MAX}^2}{MSE(x, y)}\right) \quad (22)$$

Where  $MAX$  is the maximum value of color image pixel.  $MSE(x, y)$  is the mean square error between the real underwater image and the noised image.  $(i, j)$  is the pixel value at  $(i, j)$  - th position in the image,  $i, j = 1, 2, \dots, N$ .

As a full-reference image quality evaluation index, SSIM measures image similarity from three aspects: brightness, contrast and structure. SSIM is calculated as shown in equation (23):

$$SSIM(x, y) = \frac{(2\mu_x\mu_y + c_1)(2\sigma_{xy} + c_2)}{(\mu_x^2 + \mu_y^2 + c_1)(\sigma_x^2 + \sigma_y^2 + c_2)} \quad (23)$$

Where  $\mu_x$  and  $\mu_y$  are the average values of  $x$  and  $y$ , respectively.  $\sigma_x$  and  $\sigma_y$  are the standard deviations of  $x$  and  $y$ , respectively.  $\sigma_{xy}$  is the covariance of  $x$  and  $y$ .  $c_1$  and  $c_2$  are positive constants. The larger SSIM value denotes the smaller the gap between the processed underwater image and the undistorted image, and the better denoising effect.

We first add three different Gaussian noises to the original images, i.e. Gaussian noise=0.05,0.4,0.8. The results are shown in figure 5.

For the results obtained by the four denoising methods, the PSNR and SSIM are calculated respectively, and the calculation results are shown in Table 2.

**Table 2.** Objective index calculation results

Method	PSNR	SSIM
TVM	20.1613	0.4719
WTM	21.9935	0.5147
MSRG	23.9431	0.5627
Proposed	20.2637	0.5907

From table 2, we can see that the PSNR and SSIM values of proposed method are 20.2367 and 0.5907 respectively. Its results are much higher than MSRG, WTM and TVM. Through our proposed method, different index results under different Gaussian noise are obtained as shown in tables 3-6. Meanwhile, the visualizations are also presented as shown in figures 6-9.

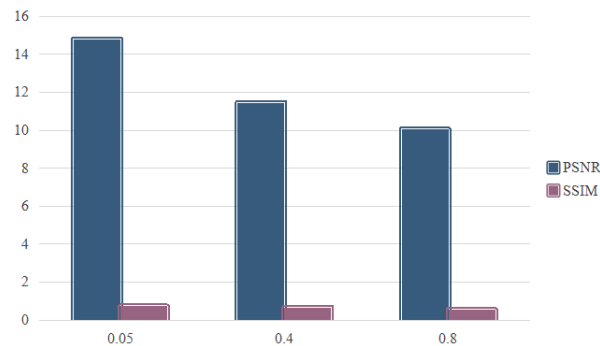


**Fig. 4.** PSNR and SSIM for image1

Figures 10-13 are the underwater image denoising results under noise with 0.05. Figures 14-17 are the underwater image denoising results under noise with 0.4.

From the above experimental results, it can be seen that, on the whole, the proposed method in this paper has a good effect on noise reduction. No matter it is the submarine tourists in Figure 10 or the fish in Figure 11, there are obvious clear signs.

## 5. Conclusions

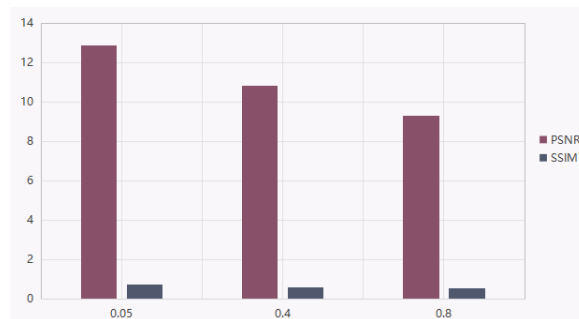
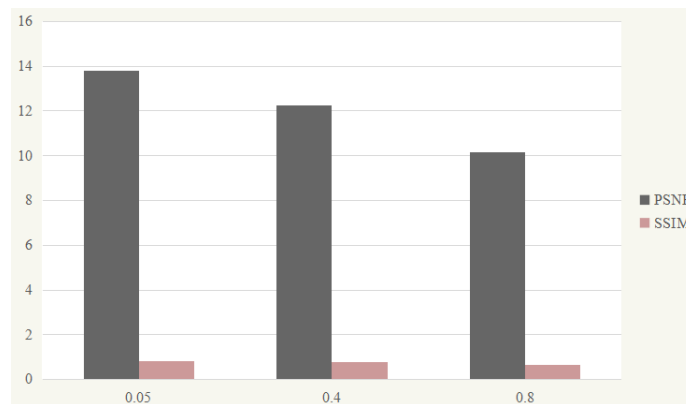
In this paper, the underwater image denoising method is studied, and an image denoising method based on curved wave filtering and 2D-VMD is proposed. Aiming at the problem that the edge of underwater image denoising is not clear and detail loss is serious, the 2D-VMD algorithm is used to achieve effective image decomposition, and the correlation

**Table 3.** Results of image2

Gaussian noise	PSNR	SSIM
0.05	13.8217	0.6693
0.4	12.7385	0.5895
0.8	9.4398	0.5467

**Table 4.** Results of image4

Gaussian noise	PSNR	SSIM
0.05	13.8172	0.8217
0.4	12.2525	0.7835
0.8	10.1654	0.6315

**Fig. 5.** PSNR and SSIM for image3**Fig. 6.** PSNR and SSIM for image4

coefficient and structural similarity are introduced to further screen the effective modal components and then the curve-wave filtering is used to obtain the denoised images with higher structural similarity, brightness, contrast, edge restoration degree and detail preservation. Effectively improve the image quality. Through experiments, the minimum peak

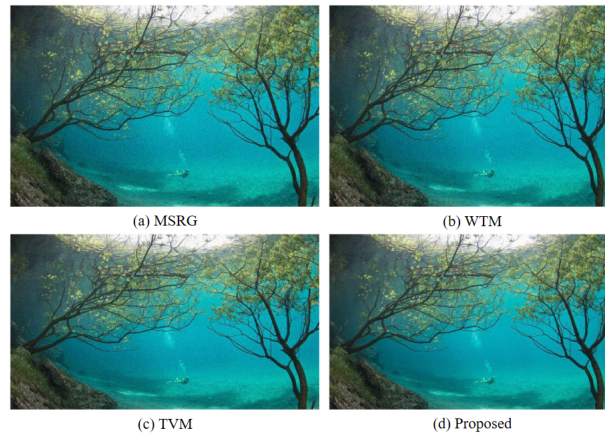


**Fig. 7.** Denoising comparison results for image1 under noise=0.05

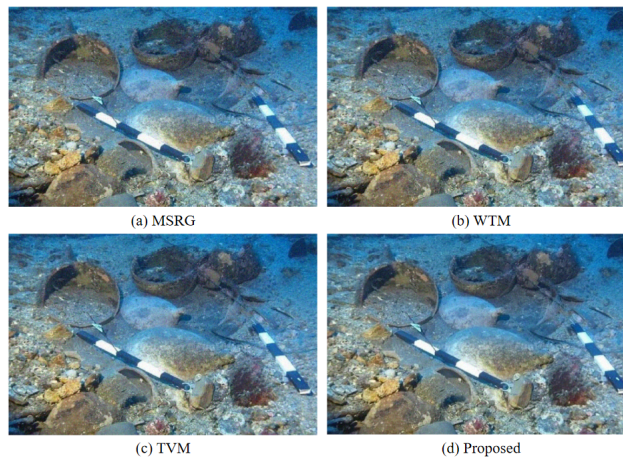


**Fig. 8.** Denoising comparison results for image3 under noise=0.05

signal-to-noise ratio (PSNR) which can be processed by the algorithm is determined. The denoising of low quality images can satisfy most of the complex conditions and provide help for the subsequent image processing tasks.

**Acknowledgments.** Authors are grateful for the anonymous review by the review experts.

## References

1. Brondi S, Neresini F, Sciandra A. The social representation of nanotechnologies and its relationships with those of science and technology: Making familiar the unfamiliar between enthusiasm and caution[J]. *Journal of Risk Research*, 2022, 25(1): 113-137.

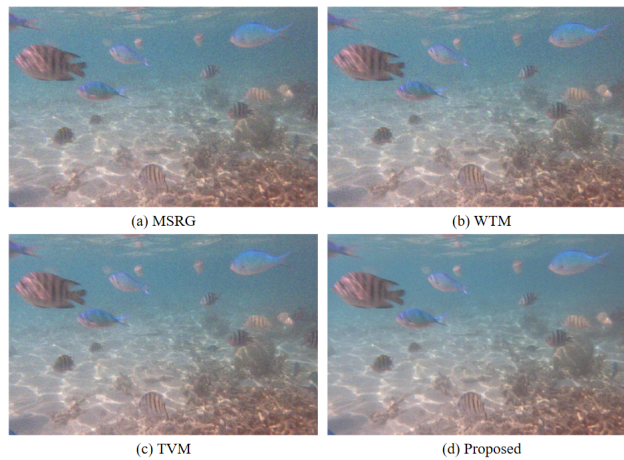


**Fig. 9.** Denoising comparison results for image4 under noise=0.05

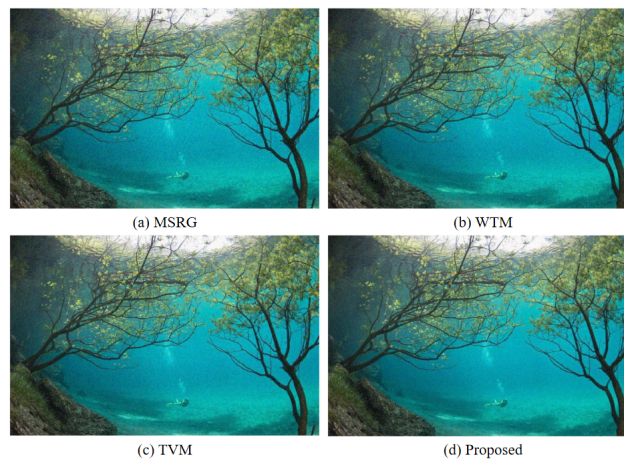


**Fig. 10.** Denoising comparison results for image1 under noise=0.4

2. He X, Ping Q, Hu W. Does digital technology promote the sustainable development of the marine equipment manufacturing industry in China?[J]. Marine policy, 2022(Feb.): 136. DOI:10.1016/j.marpol.2021.104868.
3. Wang M, Chu Y, Qiang L, et al. Rapid, amplification-free and high-throughput SARS-CoV-2 RNA detection via a reduced-graphene-oxide based fluorescence assay[J]. Sensors & Diagnostics, 2022, 1(2): 262-269.
4. Sun X, Liu L, Dong J. Underwater image enhancement with encoding-decoding deep CNN networks[C]//2017 IEEE SmartWorld, Ubiquitous Intelligence & Computing, Advanced & Trusted Computed, Scalable Computing & Communications, Cloud & Big Data Computing, Internet of People and Smart City Innovation (SmartWorld/SCALCOM/UIC/ATC/CBDCCom/IOP/SCI).IEEE, 2017. DOI:10.1109/UIC-ATC.2017.8397462.

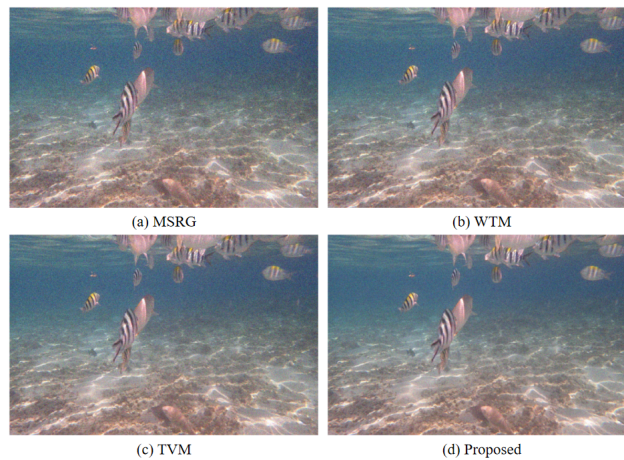


**Fig. 11.** Denoising comparison results for image2 under noise=0.4

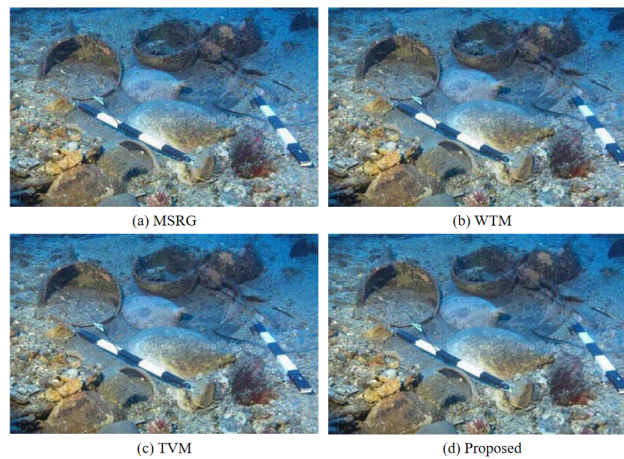


**Fig. 12.** Denoising comparison results for image3 under noise=0.4

5. Tang Z, Li J, Huang J, et al. Multi-scale convolution underwater image restoration network [J]. *Machine Vision and Applications*. vol. 33, no. 85 (2022). <https://doi.org/10.1007/s00138-022-01337-3>
6. Wang S, Li W, Xing L. A review on marine economics and management: How to exploit the ocean well[J]. *Water*, 2022, 14(17): 2626.
7. Sun Y, Yuan C, Yan X. Theoretical model research on IV characteristics of solar cell under the marine environment[C]//2015 International Conference on Transportation Information and Safety (ICTIS). IEEE, 2015: 877-882.
8. Durden J M, Schoening T, Althaus F, et al. Perspectives in visual imaging for marine biology and ecology: from acquisition to understanding[M]//*Oceanography and Marine Biology*. CRC Press, 2016: 9-80.

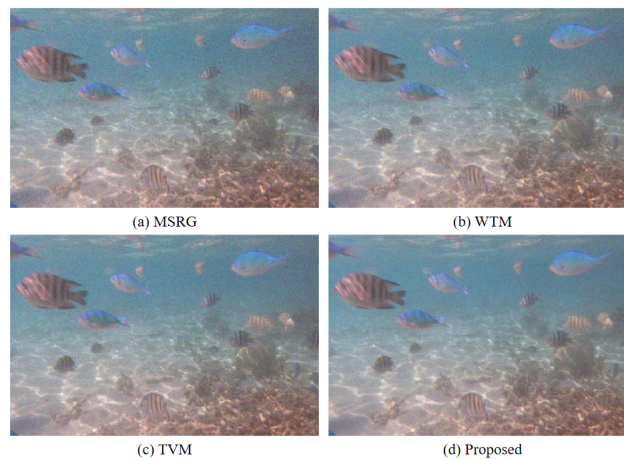


**Fig. 13.** Denoising comparison results for image4 under noise=0.4

9. Yuan X, Guo L, Luo C, et al. A survey of target detection and recognition methods in underwater turbid areas[J]. *Applied Sciences*, 2022, 12(10): 4898.
10. L. Teng et al., "FLPK-BiSeNet: Federated Learning Based on Prior Knowledge and Bilateral Segmentation Network for Image Edge Extraction," in *IEEE Transactions on Network and Service Management*, 2023. doi: 10.1109/TNSM.2023.3273991.
11. Kocak D M, Caimi F M. The current art of underwater imaging - with a glimpse of the past and vision of the future[J]. *Marine Technology Society Journal*, 2005, 39(3): 5-26.
12. Thanh D N H, Engi?no?lu S. An iterative mean filter for image denoising[J]. *IEEE Access*, 2019, 7: 167847-167859.
13. Kumar N, Dahiya A K, Kumar K. Modified median filter for image denoising[J]. *International Journal of Advanced Science and Technology*, 2020, 29(4s): 1495-1502.
14. Teng Lin, Hang Li and Shoulin Yin. Modified Pyramid Dual Tree Direction Filter-based Image De-noising via Curvature Scale and Non-local mean multi-Grade remnant multi-Grade Remnant Filter [J]. *International Journal of Communication Systems*. vol. 31, no. 16, November 10, pp. e.3486.1-e.3486.12, 2018.
15. Guo G. Real-time medical image denoising and information hiding model based on deep wavelet multiscale autonomous unmanned analysis[J]. *Soft Computing*, 2023, 27(7): 4263-4278.
16. Wang L, Xiao D, Hou W S, et al. A nonlocal enhanced Low-Rank tensor approximation framework for 3D Magnetic Resonance image denoising[J]. *Biomedical Signal Processing and Control*, 2022, 72: 103302.
17. Onur T Ö. Improved image denoising using wavelet edge detection based on Otsu's thresholding[J]. *Acta Polytechnica Hungarica*, 2022, 19(2): 79-92.
18. F. Wang, B. Yang, Y. Wang and M. Wang. Learning From Noisy Data: An Unsupervised Random Denoising Method for Seismic Data Using Model-Based Deep Learning[J]. *IEEE Transactions on Geoscience and Remote Sensing*, vol. 60, pp. 1-14, 2022, Art no. 5913314, doi: 10.1109/TGRS.2022.3165037.
19. Mu Q, Wang X, Wei Y, et al. Low and non-uniform illumination color image enhancement using weighted guided image filtering[J]. *Computational Visual Media*, 2021, 7: 529-546.
20. Y. Sun, S. Yin and H. Li. A New Wavelet Threshold Function Based on Gaussian Kernel Function for Image De-noising[J]. *Journal of Information Hiding and Multimedia Signal Processing*, Vol. 10, No. 1, pp. 91-101, January 2019.

21. Feng L, Li J, Li C, et al. A Blind Source Separation Method Using Denoising Strategy Based on ICEEMDAN and Improved Wavelet Threshold[J]. *Mathematical Problems in Engineering*, 2022, 2022.
22. K. Dragomiretskiy and D. Zosso. Variational Mode Decomposition[J]. *IEEE Transactions on Signal Processing*, vol. 62, no. 3, pp. 531-544, Feb.1, 2014, doi: 10.1109/TSP.2013.2288675.
23. Zosso D, Dragomiretskiy K, Bertozzi, A.L. et al. Two-Dimensional Compact Variational Mode Decomposition[J]. *Journal of Mathematical Imaging and Vision*, 58, 294-320 (2017). <https://doi.org/10.1007/s10851-017-0710-z>
24. Zhang X, Gu H, Zhou L, et al. Improved dual-domain filtering and threshold function denoising method for ultrasound images based on non-subsampled contourlet transform[J]. *Journal of Medical Imaging and Health Informatics*, 2017, 7(7): 1624-1628.
25. Messagier M, Meguellati S, Mahgoun H. Fringe pattern denoising using two-dimensional variational mode decomposition (2D-VMD) method for inspection of flatness of reduced surfaces[J]. *Experimental Techniques*, 2022: 1-15.
26. Khaldi A, Kafi M R, Moad M S. Wrapping based curvelet transform approach for ECG watermarking in telemedicine application[J]. *Biomedical Signal Processing and Control*, 2022, 75: 103540.
27. Nagaraja Kumar N, Jayachandra Prasad T, Prasad K S. An intelligent multimodal medical image fusion model based on improved fast discrete curvelet transform and Type-2 fuzzy entropy[J]. *International Journal of Fuzzy Systems*, 2023, 25(1): 96-117.
28. You Q, Trzasko J D, Lowerison M R, et al. Curvelet transform-based sparsity promoting algorithm for fast ultrasound localization microscopy[J]. *IEEE transactions on medical imaging*, 2022, 41(9): 2385-2398.
29. Cywińska M, Trusiak M, Zuo C, et al. Enhancing single-shot fringe pattern phase demodulation using advanced variational image decomposition[J]. *Journal of Optics*, 2019, 21(4): 045702.
30. Li Y, He D, Li Y. Underwater visual image denoising based on total variation method[C]//Conference on Infrared, Millimeter, Terahertz Waves and Applications (IMT2022). SPIE, 2023, 12565: 709-714.
31. Li C, Guo C, Ren W, et al. An underwater image enhancement benchmark dataset and beyond[J]. *IEEE Transactions on Image Processing*, 2019, 29: 4376-4389.
32. C. Li, S. Lian, J. Niu, C. Wang and X. Zhou, "Research on Underwater Image Denoising Based on Wavelet Threshold Method," 2022 7th International Conference on Intelligent Computing and Signal Processing (ICSP), Xi'an, China, 2022, pp. 1941-1947, doi: 10.1109/ICSP54964.2022.9778825.
33. Zhou J, Yao J, Zhang W, et al. Multi-scale retinex-based adaptive gray-scale transformation method for underwater image enhancement[J]. *Multimedia Tools and Applications*, 2022: 1-21.
34. Li Y, He D, Li Y. Underwater visual image denoising based on total variation method[C]//Conference on Infrared, Millimeter, Terahertz Waves and Applications (IMT2022). SPIE, 2023, 12565: 709-714.
35. Li C, Lian S, Niu J, et al. Research on Underwater Image Denoising Based on Wavelet Threshold Method[C]//2022 7th International Conference on Intelligent Computing and Signal Processing (ICSP). IEEE, 2022: 1941-1947.
36. Zhou J, Yao J, Zhang W, et al. Multi-scale retinex-based adaptive gray-scale transformation method for underwater image enhancement[J]. *Multimedia Tools and Applications*, 2022: 1-21.

**Yulong Qiao** was born in 1978. He received the Doctoral degree in engineering from the Harbin Institute of Technology in 2006. In recent years, he has published more than 50 papers in domestic and foreign journals and important conferences, among which more than

20 papers were indexed by SCI, and more than 30 were indexed by EI. His research interests include signal representation and analysis, statistical image processing, image/video processing and applications, and texture analysis and applications. He has won two science and technology awards of Heilongjiang Province. He is a Senior Member of the Chinese Institute of Electronics and IEEE Signal Processing Branch.

**Lin Teng** received the M.A. degree from Shenyang Normal University, Shenyang, China, in 2020. She is currently pursuing the Ph.D. degree with the College of Information and Communication Engineering, Harbin Engineering University, Harbin. Her research interests are image processing and semantic segmentation.

**Shoulin Yin** received the M.A. degree from Shenyang Normal University, Shenyang, China, in 2015. He is currently pursuing the Ph.D. degree with the College of Information and Communication Engineering, Harbin Engineering University, Harbin. His research interests are remote sensing image processing and object detection.

*Received: March 14, 2024; Accepted: June 29, 2024.*

